Available online at www.sciencedirect.com

SciVerse ScienceDirect

Ceramics International 38 (2012) 1115–1126

CERAMICS INTERNATIONAL

www.elsevier.com/locate/ceramint

Effects of loading rate and temperature on domain switching and evolutions of reference remnant state variables during polarization reversal in a PZT wafer

Najae Lee, Sang-Joo Kim *

Department of Mechanical and Information Engineering, University of Seoul, Dongdaemun-gu, Seoul, 130-743, Republic of Korea

Received 14 July 2011; received in revised form 17 August 2011; accepted 17 August 2011
Available online 26 August 2011

Abstract

A PZT wafer poled in thickness direction is subject to through-thickness electric field cyclic loads at four different loading rates and four different temperatures. Electric displacement in thickness direction and in-plane extensional strain are measured and plotted during a complete cycle of polarization reversal. Reference remnant polarization and reference remnant in-plane extensional strain are calculated from the measured data. Effects of electric field loading rate and temperature on domain switching process and evolutions of reference remnant state variables are discussed and explained using consecutive two step slow 90° domain switching processes and reduced coercive field at high temperatures.

Keywords: D. PZT; Polarization reversal; Switching; Remnant; Loading rate; Temperature

1. Introduction

Ferroelectric ceramics, e.g. lead titanate zirconate (PZT), have excellent electromechanical properties such as excellent electromechanical coupling, prompt response, low power consumption, and so on. The materials are classified as two groups according to their properties: soft and hard materials. Soft materials have relatively higher piezoelectric constants such as higher sensitivity and permittivity because of its high domain mobility. Thus it suits various sensor and low power generator. Hard materials have relatively lower piezoelectric constants. It is strong enough to withstand high levels of mechanical and electrical loading. Hence, it can be applied to high power applications; for example, high voltage or high power generators and transducers. In all these applications, the materials are often subject to strong electric fields at high temperatures. Strong electric fields at high temperatures induce unnecessary domain switching and nonlinearity in the materials and thereby the performance of piezoelectric devices may be deteriorated. In order to design efficient and reliable piezoelectric devices, it is necessary to develop the constitutive models that can predict the nonlinear behavior of the materials at strong electric fields and high temperatures [1–5]. The construction of constitutive models should be based on correct understanding of domain switching behavior at strong electric fields and high temperatures.

Recently, much experimental work has been carried out to understand switching mechanisms in the materials and to provide experimental data needed for the construction of constitutive models. Nonlinear electromechanical coupling behavior has been measured and discussed by Cao and Evans [6] and Lynch [7]. Zhou [8] measured the polarization and strain (in poling direction) responses of a PZT ceramic under electric field cyclic loads of different rates and analyzed the effects of loading rate using different speeds of 90° and 180° switching. Constant permittivity and linear dependency of piezoelectric coefficient on remnant polarization of a PZT ceramic under unipolar electrical loading have been shown experimentally by Selten et al. [9]. Evolutions of linear elastic, dielectric, and piezoelectric moduli of a ferroelectric ceramic during electro-mechanical loading at a constant temperature have been measured by Liu and Huber [10]. Dependency of permittivity and piezoelectric coefficient on remnant polarization and temperature has been measured and evaluated during polarization reversal of a PZT wafer [11]; state-dependent

* Corresponding author. Tel.: +82 2 2210 2757; fax: +82 2 2210 5575.
E-mail address: sangjookim@gmail.com (S.-J. Kim).

0272-8842/$36.00
doi:10.1016/j.ceramint.2011.08.039

pyroelectric and thermal expansion coefficients have also been measured and proposed as a function of remnant state variables and temperature [12]; macroscopic comparisons of domain switching processes of a PZT wafer under constant electric fields at various temperatures have been made using reference remnant state variables [13,14].

In present work, a PZT wafer is poled in thickness direction is subject to through-thickness electric field cyclic loads that increase and decrease at four different constant rates and four different temperatures. Electric displacement in thickness direction and in-plane extensional strain are measured during electric field cyclic loading. Evolutions of various linear moduli during polarization reversal induced by electric field cyclic loads are either evaluated from measured electric displacement and in-plane strain data or taken from previous reports [11–14]. By subtracting linear contributions of electric field and thermal contributions from measured data, the so-called reference remnant polarization and reference remnant in-plane extensional strain are calculated. Characteristics of nonlinear behavior of the materials are discussed and analyzed using evolutions of calculated reference remnant polarization and in-plane strain state variables. Consecutive two step 90° domain switching and reduced coercive field at high temperatures are used to explain loading rate- and temperature-dependent behavior of the materials. Two- and one-dimensional schematic diagrams of domain distribution corresponding to each important state during polarization reversal were proposed based on consecutive two step 90° domain switching. Experimental observations and discussion made in the present work will be useful in constructing reliable macroscopic constitutive models for nonlinear behavior of ferroelectric ceramics.

2. Experiment

A commercially available soft PZT wafer (3203HD, CTS, USA) of dimensions 71 mm × 23 mm × 0.5 mm is used as a specimen for experiments. The specimen PZT wafer is commonly used for medical ultrasound devices, inkjet printing, and hard disk drive markets. According to the manufacturing company (www.ctscorp.com/components/pzt/supmat.asp), the Curie point of wafer is 225 °C, the coupling coefficients are $k_{31} = 0.43$ and $k_{33} = 0.75$, and the piezoelectric charge coefficients are $d_{31} = -320 \times 10^{-12}$ m V^{-1} and $d_{31} = 650 \times 10^{-12}$ m V^{-1}. The longitudinal, transverse, and thickness directions of wafer are designated as x_1, x_2, and x_3, respectively. They are also often called as 1, 2, and 3 directions, respectively. Initially, a PZT wafer is poled in $-x_3$ direction and it is subject to twelve cycles of electric field loading between $E_3 = -2$ and 2 MV m^{-1} in thickness direction at each of four temperatures 20, 50, 80, and 110 °C For each three cycles of loading at a constant temperature, the rate of applied electric field increases from 0.01 to 0.1, 1, and then finally to 10 MV m^{-1} s^{-1}.

Measurements are made during the last cycle among three cycles of a given loading rate. The sampling rate is 500 Hz. During electric field-induced polarization reversals, the wafer remains isotropic with respect to thickness direction and thus the in-plane extensional strain of the wafer is the same in the longitudinal and transverse directions of the wafer. In the present paper, the in-plane extensional strain is denoted as S_1. Four strain gauges are attached in both sides of the wafer specimen and they are averaged to evaluate in-plane strain S_1 of the wafer. The used strain gauges are fully encapsulated constantan strain gauges (WA-03-062TT-350, VISHAY, Germany). Electric displacement in thickness direction is measured using a Sawyer-Tower bridge, where a reference capacitor (metalized polypropylene capacitor) of capacitance 120 μF is connected to the specimen in series. This is 1200 times larger than the PZT specimen capacitance 0.1 μF. The voltage across the reference capacitor is measured by a Keithley 6514 electrometer. Discharge circuits are added to the system to remove the charges accumulated in the PZT specimen and the reference capacitor during experiments. All equipment output signals pass through a data acquisition board (PCI 6221, National Instruments, TX, USA) and are manipulated using a LABVIEW software.

In each initial poled state before loading, strain gauges are set to be zero and discharge circuits are activated to remove unnecessary charges accumulated in the system. In-plane extensional strain and electric displacement data measured during the last cycle of loading in each of four loading rates and four temperatures are taken, manipulated, and displayed in next chapter to understand and explain rate- and temperature-dependent behavior of electric field-induced polarization reversal using remnant state variables and 90° domain switching.

3. Results and discussion

3.1. Measured polarization hysteresis and strain butterfly responses

Electric displacement in thickness direction D_3 and in-plane extensional strain S_1 of a PZT wafer are measured during polarization reversal induced by through-thickness electric field E_3 whose magnitude increases and then decreases between −2 and 2 MV m^{-1} at four constants rates of 0.01, 0.1, 1, and 10 MV m^{-1} s^{-1}. The four loading rates correspond to 0.00125, 0.0125, 0.125, and 1.25 Hz, respectively. All measurements are made at four temperatures 20, 50, 80, and 110 °C. Measured data are plotted over electric field for one complete cycle of polarization reversal in Figs. 1 and 2. Figs. 1(a) and 2(a) show measured electric displacement hysteresis responses, and Figs. 1(b) and 2(b) show in-plane extensional strain butterfly responses of the wafer. The effects of temperature at each constant loading rate are shown in Fig. 1. In Fig. 1(a), it is clear that both the coercive field and the magnitude of remnant polarization at zero electric field decrease with increasing temperature at each of the four loading rates of electric field, which agrees with the experimental observations of Chong [15], Kounga et al. [16], and Wongdamnern et al. [17] and with the theoretical predictions of Smith and Hom [18] and Mauck and Lynch [19]. The magnitude of in-plane strain is observed to increase with temperature for all range of electric field in

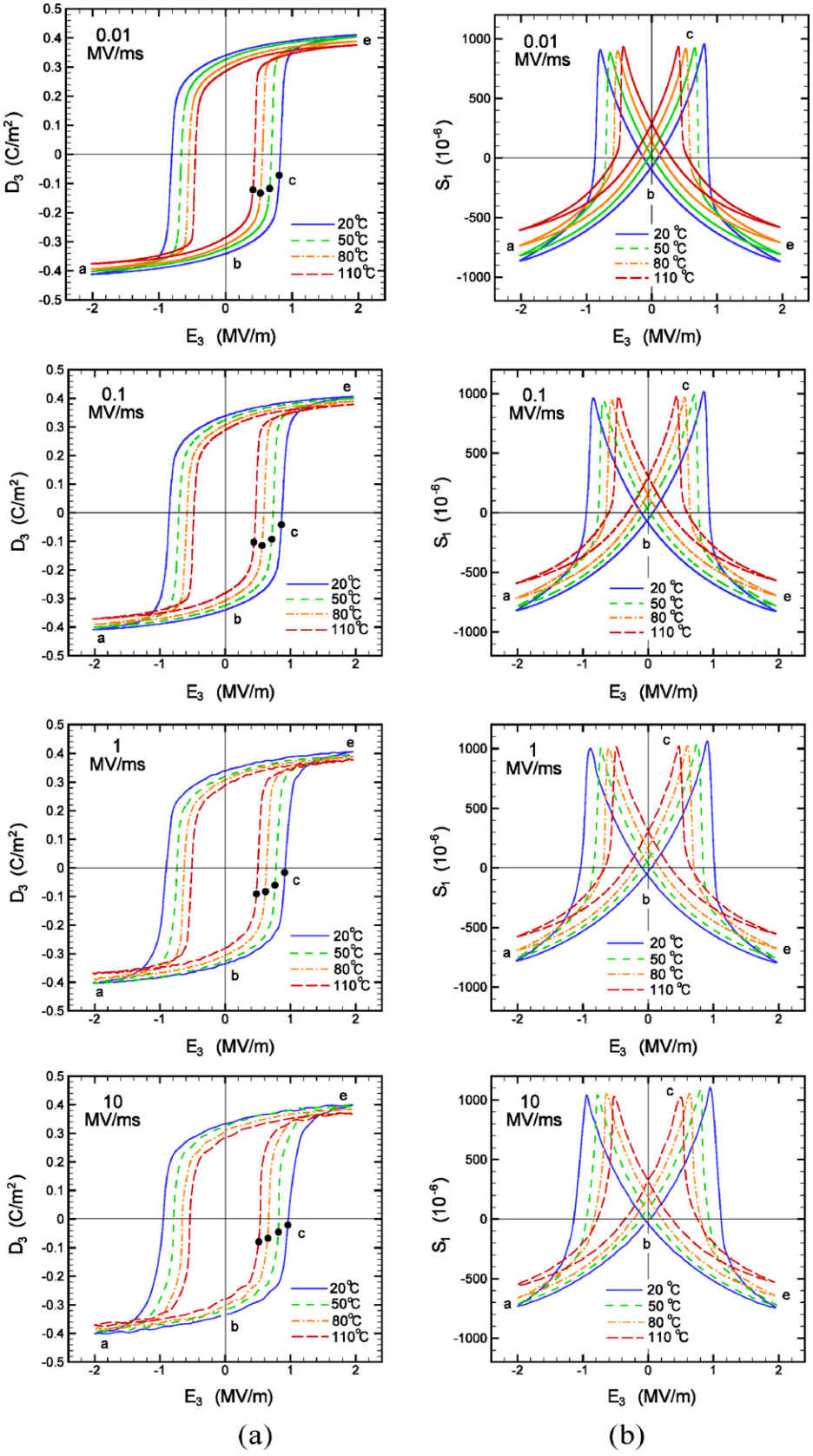

Fig. 1. Responses of a PZT wafer under through-thickness electric field cycling of ±2 MV m^{-1} at each of four loading rates 0.01, 0.1, 1, and 10 MV m^{-1} s^{-1}. At each loading rate, responses at four temperatures 20, 50, 80, and 110 °C are drawn as solid, dashed, dashed and dotted, and long-dashed lines, respectively. (a) Electric displacement hysteresis responses and (b) in-plane extensional strain butterfly responses.

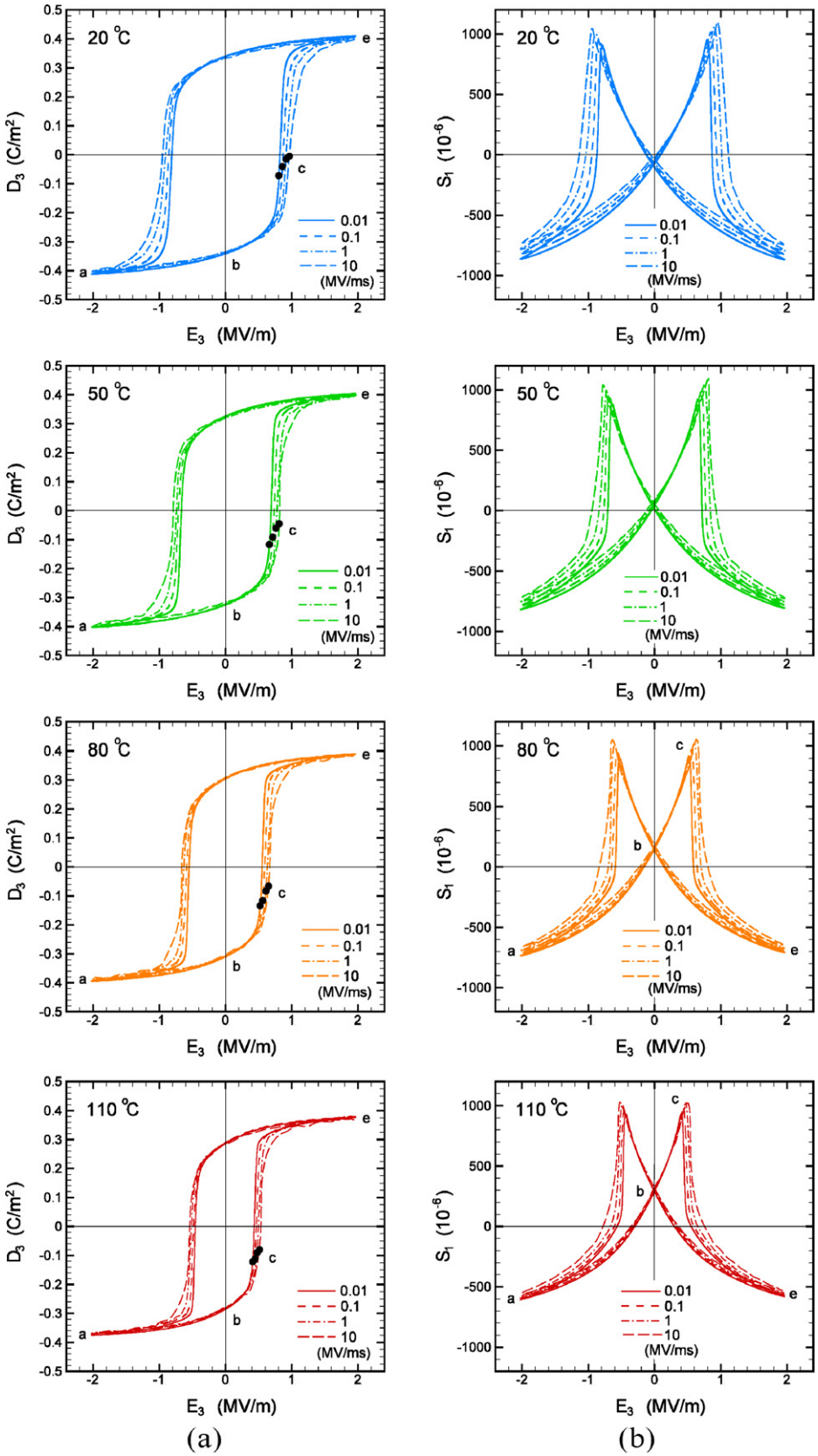

Fig. 2. Responses of a PZT wafer under through-thickness electric field cycling of ±2 MV m^{-1} at each of four temperatures 20, 50, 80, and 110 °C. At each temperature, responses at four loading rates 0.01, 0.1, 1, and 10 MV m^{-1} s^{-1} are drawn as solid, dashed, dashed and doted, and long-dashed lines, respectively. (a) Electric displacement hysteresis responses and (b) in-plane extensional strain butterfly responses.

Fig. 1(b), though the maximum value of in-plane strain is approximately the same at all four temperatures. The observed increase in in-plane strain with temperature is due to thermal expansion effect. Fig. 2(a) and (b) shows the effects of loading rate on polarization hysteresis and strain butterfly responses, respectively, at each of four constant temperatures. It is shown in Fig. 2(a) that coercive field increases with electric field loading rate at all four temperatures, which was simulated by theoretical models [4,20] and observed by experiments [21]. The magnitudes of remnant polarization and remnant in-plane strain at zero electric field are approximately the same regardless of loading rates at each constant temperature. However, the magnitude of in-plane strain over all range of applied electric field in the figure seems to increase with loading rate at each constant temperature. This can be attributed to slow 90° domain switching at fast electric field loading rates, which will be discussed later in more detail.

3.2. State-dependent linear moduli and remnant state variables

A PZT wafer that is poled in thickness direction is subject to cyclic loading of through-thickness electric field E_3. Since the PZT wafer is composed of different types of variants and each type of variant has different material properties, the values of various linear moduli of the wafer such as pyroelectric or piezoelectric coefficients change during polarization reversal induced by electric field loading cycle. It is useful to describe the complicated internal domain structure of the wafer by two macroscopic state variables: reference remnant polarization in thickness direction P_3^{R0} and reference remnant in-plane strain S_1^{R0}. The two reference remnant state variables P_3^{R0} and S_1^{R0} can be calculated from the piezoelectric equations for a PZT wafer with state-dependent linear moduli [11,13,14]

$$\begin{aligned} D_3 &= \hat{\kappa}_3^{T,\theta}(\theta)\, E_3 + \hat{p}_3^{T}(P_3^R,\theta)\,(\theta-\theta_0) + P_3^{R0},\\ S_1 &= \hat{d}_{31}^{\theta}(P_3^R,\theta)\, E_3 + \hat{\alpha}_1^{E}(P_3^R,\theta)\,(\theta-\theta_0) + S_1^{R0}, \end{aligned} \tag{1}$$

where $\hat{\kappa}_3^{T,\theta}(\theta)$ is permittivity in thickness direction at constant stress and temperature, $\hat{p}_3^{T}(P_3^R,\theta)$ pyroelectric constant in thickness direction at constant temperature, $\hat{d}_{31}^{\theta}(P_3^R,\theta)$ piezoelectric coefficient at constant temperature relating in-plane extensional strain S_1 to through-thickness electric field E_3, $\hat{\alpha}_1^{E}(P_3^R,\theta)$ thermal expansion coefficient in in-plane direction at constant electric field, and P_3^{R0} and S_1^{R0} are reference remnant polarization and reference remnant in-plane extensional strain, respectively. Remnant polarization P_3^R and remnant in-plane strain S_1^R are obtained by subtracting linear electric displacement and piezoelectric strain, both of which are proportional to electric field, from measured electric displacement and in-plane strain, respectively. Thus, from Eq. (1), they are given by

$$\begin{aligned} P_3^R &= \hat{p}_3^{T}(P_3^R,\theta)\,(\theta-\theta_0) + P_3^{R0},\\ S_1^R &= \hat{\alpha}_1^{E}(P_3^R,\theta)\,(\theta-\theta_0) + S_1^{R0}. \end{aligned} \tag{2}$$

According to previous experiments on a PZT wafer [11], permittivity $\hat{\kappa}_3^{T,\theta}(\theta)$ in Eq. (1) remains approximately constant during polarization reversal but it depends on temperature linearly. They evaluated permittivity at the state of zero electric field marked as point b in Fig. 3, where the polarization hysteresis responses of the wafer at 0.01 MV m^{-1} s^{-1} are plotted at 20 and 110 °C. However, in the present paper, permittivity is evaluated at the state of maximum electric field marked as e in the figure so that the effect of domain switching is not included in the evaluation of permittivity. It is found from present experiments that permittivity evaluated at point e is almost constant independent of temperature. Thus we get $\kappa_3^{T,\theta} = 1.685\times10^{-8}$ C V^{-1} m^{-1}. Pyroelectric constant $\hat{p}_3^{T}(P_3^R,\theta)$ was proposed as a function of remnant polarization P_3^R and temperature θ [12]

$$\hat{p}_3^{T}(P_3^R,\theta) = p_3^{T,sat}\frac{P_3^R}{\hat{P}_3^{R,sat}(\theta)}, \tag{3}$$

where $p_3^{T,sat}$ is pyroelectric coefficient evaluated at the saturated state corresponding to zero electric field and $\hat{P}_3^{R,sat}(\theta)$ the value of remnant polarization evaluated at the saturated state of zero electric field given as a function of temperature. Thus $\hat{P}_3^{R,sat}(\theta)$ is given as

$$\hat{P}_3^{R,sat}(\theta) = p_3^{T,sat}\,(\theta-\theta_0) + P_3^{R0,sat}, \tag{4}$$

and we get from measurements that $p_3^{T,sat} = -6.08\times10^{-4}$ C m^{-2} °C^{-1} and $P_3^{R0,sat} = 0.341$ C m^{-2}. Similarly, remnant polarization at the state of maximum electric field in the figures is evaluated at point e, as shown in the top of Fig. 3. It is given as a function of temperature by

$$\hat{P}_3^{R,\max}(\theta) = p_3^{T,\max}\,(\theta-\theta_0) + P_3^{R0,\max}, \tag{5}$$

where $P_3^{R0,max} = 0.380$ C m^{-2} and $p_3^{T,max} = -3.87\times10^{-4}$ C m^{-2} °C^{-1} can be obtained from measurements. Piezoelectric coefficient $\hat{d}_{31}^{\theta}(P_3^R,\theta)$ in Eq. (1) was proposed as a function of remnant polarization and temperature by Kim and Kim [11] and Kim et al. [13], where it is based on piezoelectric coefficient evaluated at the saturated state of zero electric field. In the present work, it is based on piezoelectric coefficient evaluated at the state of maximum electric field marked e in Fig. 3. Then we get

$$\hat{d}_{31}^{\theta}(P_3^R,\theta) = \hat{d}_{31}^{\theta,\max}(\theta)\frac{P_3^R}{\hat{P}_3^{R,\max}(\theta)}, \tag{6}$$

where $\hat{d}_{31}^{\theta,max}(\theta)$ is piezoelectric coefficient evaluated at point e, as shown in the middle of Fig. 3. It is found that $d_{31}^{\theta,max}$ is constant independent of temperature and has the value of $d_{31}^{\theta,max} = -1.88\times10^{-10}$ mV^{-1} °C^{-1}. Thermal expansion coefficient $\hat{\alpha}_1^{E}(P_3^R,\theta)$ in Eq. (1) was proposed as a function of remnant polarization P_3^R and temperature θ [12], which is

$$\hat{\alpha}_1^{E}(P_3^R,\theta) = (\alpha_1^{E,sat}-\alpha_1^{E,0})\left(\frac{P_3^R}{\hat{P}_3^{R,sat}(\theta)}\right)^2 + \alpha_1^{E,0}, \tag{7}$$

where $\alpha_1^{E,sat}$ and $\alpha_1^{E,0}$ are thermal expansion coefficients evaluated at the saturated state of zero electric field and at the state of zero remnant polarization, respectively. From measured responses, we get $\alpha_1^{E,sat} = 4.49\times10^{-6}$ °C^{-1}. The value of

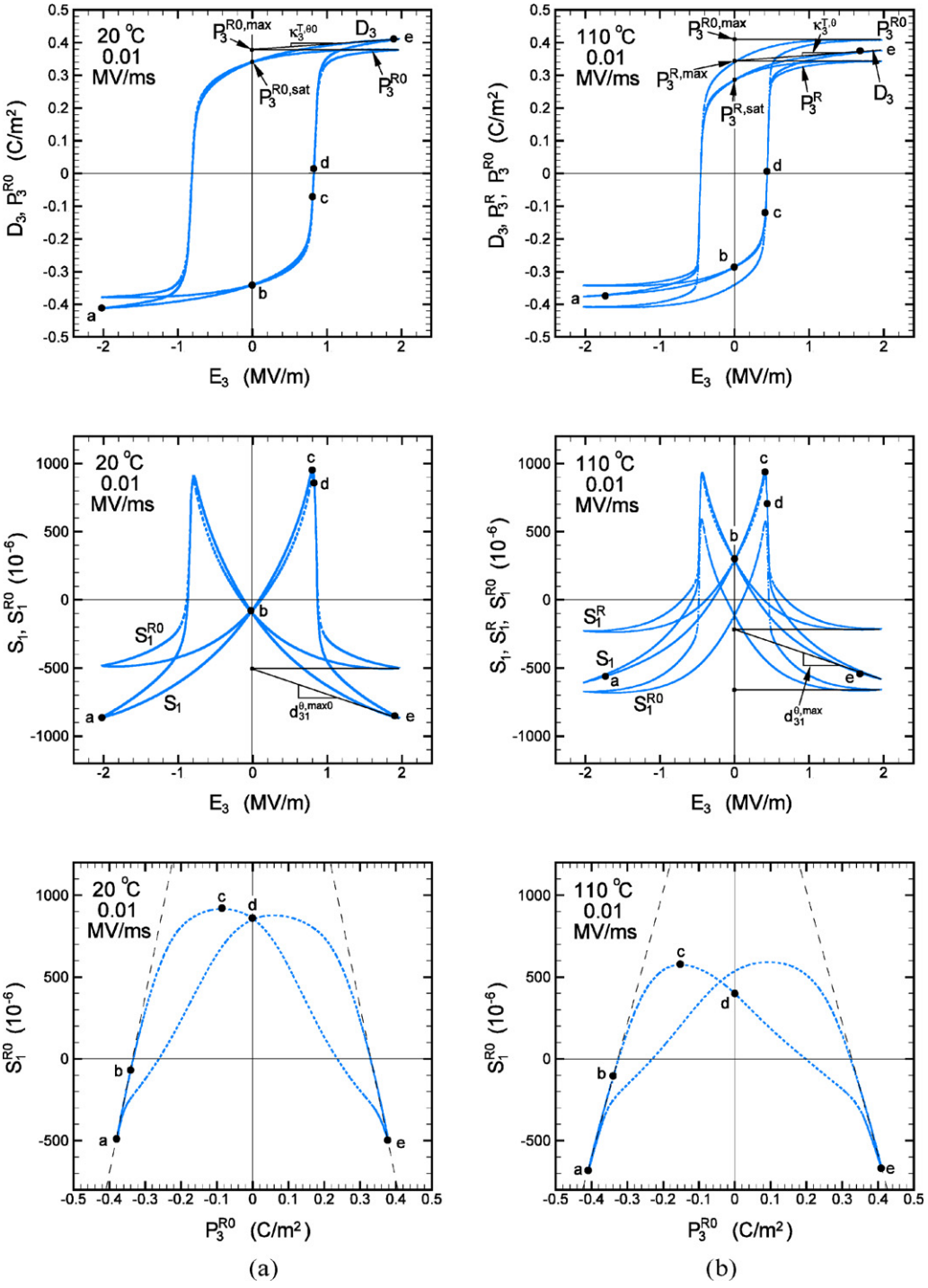

Fig. 3. Measured responses and calculated remnant state variables of a PZT wafer during electric field cycling at (a) 20 °C and 0.01 MV m^{-1} s^{-1} and (b) 110 °C and 0.01 MV m^{-1} s^{-1}. From top, electric displacement and reference remnant polarization versus electric field curves, in-plane strain and reference remnant in-plane strain versus electric field curves, and reference remnant polarization versus reference remnant in-plane strain curves.

$\alpha_1^{E,0}$ is taken from Kim and Kim [12] and it is given by $\alpha_1^{E,0} = 3.45 \times 10^{-6}\,°C^{-1}$.

Now we are ready to calculate reference remnant polarization P_3^{R0} and reference remnant in-plane strain S_1^{R0} using Eqs. (1)–(7). The procedure is as follows. First, remnant polarization P_3^R is calculated from $P_3^R = D_3 - \hat{\kappa}_3^{T,\theta}(\theta)E_3$ in Eq. $(1)_1$. Then the value of P_3^R is inserted into Eqs. (3), (6) and (7) to calculate pyroelectric coefficient p_3^T, piezoelectric coefficient d_{31}^{θ}, and thermal expansion coefficient α_1^E, respectively. The calculated piezoelectric coefficient is inserted into Eq. $(1)_2$ and remnant in-plane strain S_1^R is obtained from $S_1^R = S_1 - \hat{d}_{31}^{\theta}(P_3^R, \theta)E_3$. Then, pyroelectric and thermal expansion coefficients are inserted into Eq. (2), finally yielding reference remnant polarization P_3^{R0} and reference remnant in-plane strain S_1^{R0}.

At reference temperature 20 °C, reference remnant polarization P_3^{R0} is numerically equal to remnant polarization P_3^R, that is, $P_3^R = P_3^{R0}$ at 20 °C. Evolutions of D_3, P_3^{R0} and S_1, S_1^{R0} over electric field at 20 °C and 0.01 MV m^{-1} s^{-1} are plotted in Fig. 3(a), and evolutions of D_3, P_3^R, P_3^{R0} and S_1, S_1^R, S_1^{R0} at 110 °C and 0.01 MV m^{-1} s^{-1} in Figs. 3(b). At the bottom of Fig. 3, P_3^{R0} versus S_1^{R0} curves are drawn for two temperatures 20 and 110 °C. Reference remnant variables P_3^{R0} and S_1^{R0} can be interpreted as state variables that are associated with micro structural arrangements of domains in the wafer. Reference remnant polarization P_3^{R0} is associated with arrangement of domains in thickness direction of the wafer; reference remnant in-plane strain S_1^{R0} with arrangement of domains in in-plane directions of the wafer. Five points from a to e are marked along the switching curve from −2 to +2 MVm^{-1} in the bottom of Fig. 3. Point a is where P_3^{R0} (or S_1^{R0}) has the smallest value, point b is where electric field is zero during polarization reversal, point c is where S_1^{R0} reaches its maximum, point d is where P_3^{R0} is zero, and point e is where P_3^{R0} (or S_1^{R0}) has the largest (or smallest) value. In the figure, a dashed straight line is drawn from a to b, where S_1^{R0} is proportional to P_3^{R0}. A similar dashed line of the same magnitude of slope is drawn in point e. It is believed that only first step forward 90° domain switching occurs near point a and second step backward 90° switching near point e along each of the two dashed straight lines, respectively. At maximum S_1^{R0} point c, the amount of domains more parallel to in-plane directions of the wafer reaches its maximum during a complete cycle of polarization reversal. At point d, net polarization in thickness direction of the wafer is zero. Previous reports of Gerthsen and Kruger [22], Schmidt [23], and Kruger [24] proposed that first step forward 90° domain switching occurs from b to c and after point c, second step forward 90° domain switching is dominant. Similar discussions were made by Zhou [8].

Measured and manipulated responses at 110 °C and 0.01 MV m^{-1} s^{-1} are plotted in Fig. 3(b). It is seen that remnant polarization P_3^R has smaller magnitude but reference remnant polarization P_3^{R0} has larger magnitude than electric displacement D_3 due to pyroelectric effect. Similarly, reference remnant in-plane strain S_1^{R0} has lower value than measured in-plane strain S_1 over all range of electric field due to thermal expansion effect. It is interesting that at minimum P_3^{R0} point a, electric field has already passed through its minimum value and is a little larger than that. That is, the minimum P_3^{R0} state at point a does not coincide with the state at minimum electric field. Comparing two P_3^{R0}–S_1^{R0} curves in the bottom of Fig. 3, one can see that maximum value of S_1^{R0} at point c is lower at 110 °C than

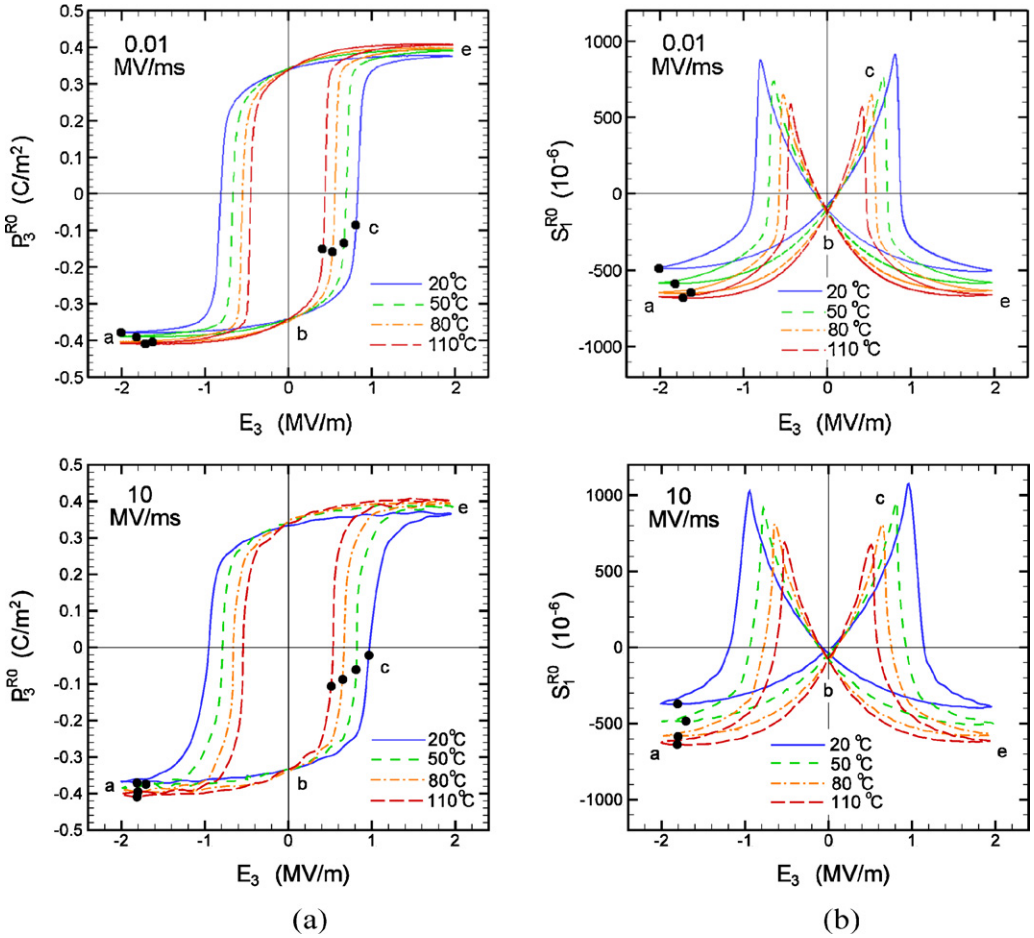

Fig. 4. Evolutions of calculated reference remnant state variables at four temperatures 20, 50, 80, and 110 °C, which are represented as solid, dashed, dashed and dotted, and long-dashed lines, respectively, during electric field cycling at 0.01(top) and 10 MV m^{-1} s^{-1} (bottom). (a) Reference remnant polarization versus electric field curves and (b) reference remnant in-plane strain versus electric field curves.

that at 20 °C. It means that less amount of domains is arranged in in-plane directions of the wafer at higher temperatures during polarization reversal. More detail discussions will be made in next section.

3.3. Effects of loading rate and temperature on domain switching process

The calculated reference remnant polarization and in-plane strain in the previous section are plotted over electric field in Figs. 4 and 5. In Fig. 4, $P_3^{R0}-E_3$ and $S_1^{R0}-E_3$ curves at four temperatures are plotted together for each of two constant loading rates 0.01 and 10 MV m^{-1} s^{-1}; in Fig. 5, the curves at four electric field loading rates are plotted for each of two temperatures 20 and 110 °C. Thus effects of temperature can be observed in Fig. 4 whereas those of loading rate in Fig. 5. Fig. 6 shows $P_3^{R0}-S_1^{R0}$ curves at each constant loading rate on the left and at each constant temperature on the right of the figure. In all figures from Figs. 4 to 6, maximum S_1^{R0} point c is marked as a solid circle symbol, which can be found clearly from measured and calculated data. In Figs. 4 and 5, minimum P_3^{R0} (or minimum S_1^{R0}) point a is also marked as a solid circle symbol, though it is not found as clearly as point c in calculated data. $P_3^{R0}-E_3$ and $S_1^{R0}-E_3$ curves for four temperatures at each constant loading rate are drawn together in the left and right of Fig. 4, respectively. In both loading rates of 0.01 and 10 MV m^{-1} s^{-1}, the curves at four temperatures pass through the same point at zero electric field marked as b in the figure. It is because evolutions of pyroelectric and thermal expansion coefficients during polarization reversal are based on their values at the saturated state of zero electric field in Eqs. (3) and (7), respectively. That is, $p_3^{T,sat}$ and $\alpha_1^{E,sat}$ are measured while the wafer specimen is heated at $P_3^R = P_3^{R,sat}$ under zero electric field. As temperature increases, the magnitudes of P_3^{R0} at large magnitudes of electric field increase in Fig. 4(a) and the values of maximum and minimum S_1^{R0} get smaller over the entire range of electric field in Fig. 4(b). Larger magnitudes of P_3^{R0} near maximum electric fields indicate that more domains are aligned in thickness direction of the wafer near the maximum electric fields; smaller values of S_1^{R0} over the entire range of electric field mean that smaller amount of domains are orientated parallel to in-plane directions of the wafer during the whole polarization reversal. The latter is not in contradiction with the former, because smaller amount of domains parallel to

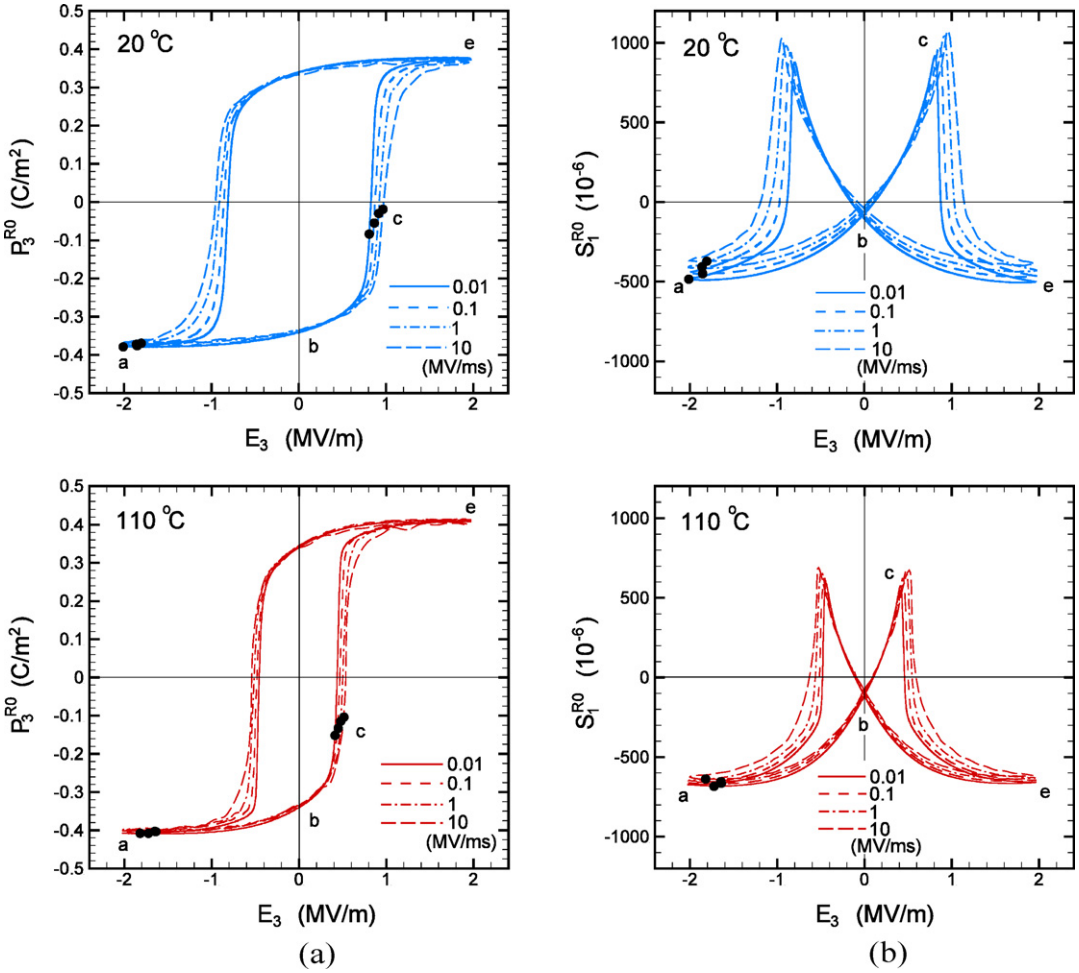

Fig. 5. Evolutions of calculated reference remnant state variables at four loading rates 0.01, 0.1, 1, and 10 MV m^{-1} s^{-1}, which are represented as solid, dashed, dashed and dotted, and long-dashed lines, respectively, during electric field cycling at 20(top) and 110 °C (bottom). (a) Reference remnant polarization versus electric field curves and (b) reference remnant in-plane strain versus electric field curves.

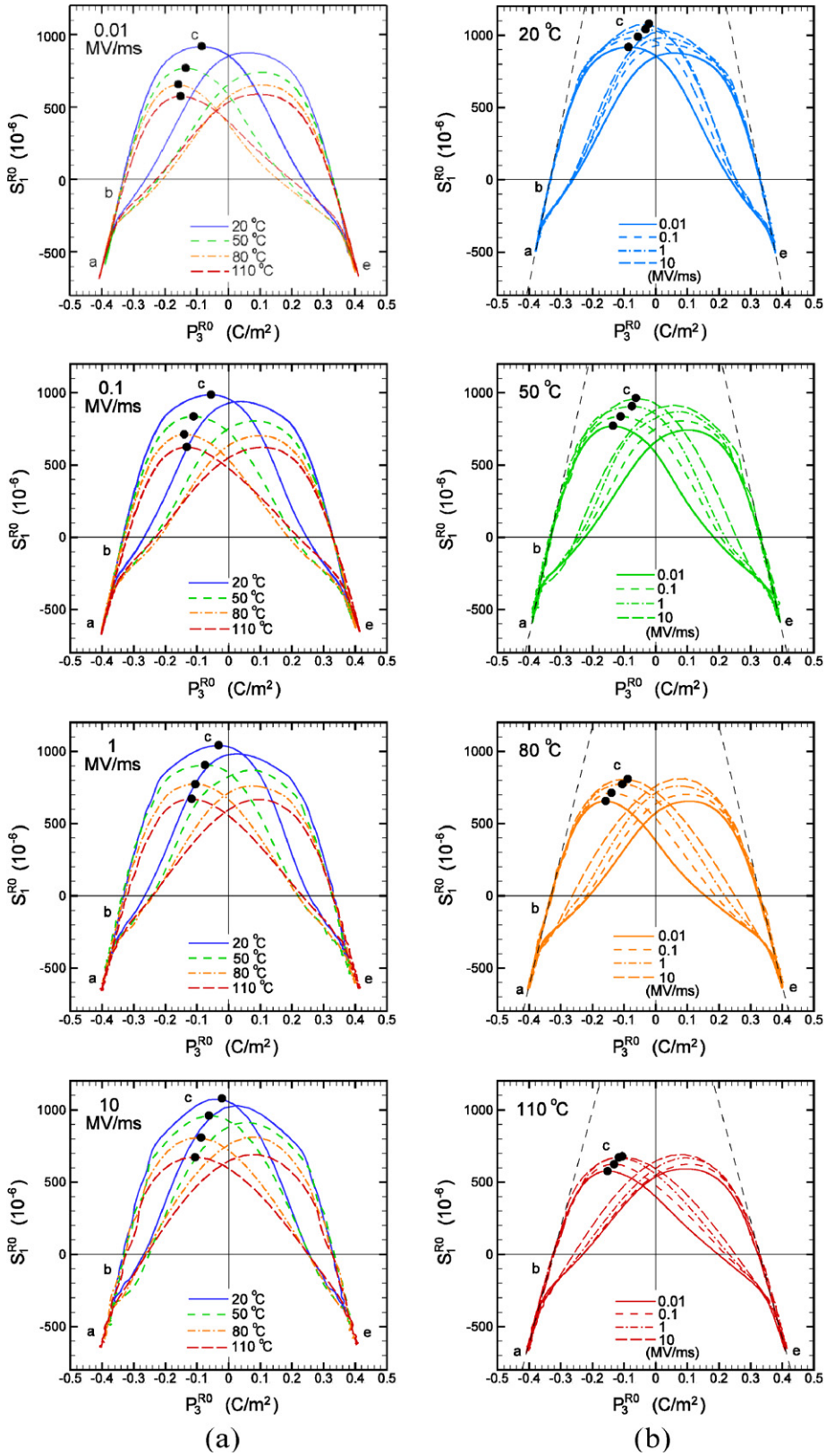

Fig. 6. Reference remnant in-plane strain versus reference remnant polarization curves (a) at each constant loading rate showing the effect of temperature and (b) at each constant temperature showing the effect of loading rate. Maximum reference remnant in-plane strain point c is marked as solid circle symbol.

in-plane directions of the wafer naturally results in larger amount of domains in thickness direction of the wafer. Therefore, it may be concluded that more domains are orientated parallel to thickness direction of the wafer at higher temperatures during an electric field-induced polarization reversal. How can one understand this effect of temperature on the evolution of domain structure? The magnitude of coercive field decreases with increasing temperature in Fig. 1(a). At higher temperatures, even the same magnitude of electric field gets more powerful in driving domain switching and polarization reversal becomes more complete. The period of time during which domains stay polarized in thickness direction of the wafer gets longer at higher temperatures, resulting in larger magnitudes of P_3^{R0} near maximum electric fields and smaller values of S_1^{R0} over the entire range of electric field, as shown in Fig. 4.

Effects of loading rate on evolutions of reference remnant variables during polarization reversal are shown in Fig. 5. With increasing loading rate, the magnitude of P_3^{R0} decreases near points a and e but that of S_1^{R0} increases over the entire range of electric field at both temperatures of 20 and 110 °C in the figure. That is, P_3^{R0} decreases but S_1^{R0} increases with increasing loading rate. This can be explained by relatively slow 90° domain switching. At relatively fast loading rates, 90° domain switching does not follow applied electric field and always lags behind it. As a result, more domains stay arranged near in-plane directions of the wafer, resulting in smaller P_3^{R0} and larger S_1^{R0} at faster loading rates. It is interesting to locate point a with the smallest values of P_3^{R0} and S_1^{R0} in Figs. 4 and 5, though their locations were not clearly defined in calculated data files. One can see in the figures that electric field at point a has the smallest value at 20 °C and 0.01 MV m^{-1} s^{-1}, whereas it does not, in general, at other temperatures and loading rates. That is, in case of higher temperatures or faster loading rates, point a moves rightward in the plane of the figure, thus P_3^{R0} reaching its minimum a little after electric field hits its minimum. A possible explanation can also be made by using relatively slow 90° domain switching. At higher temperatures or faster loading rates, the ability of electric field for driving domain switching gets bigger. However, since the rate of 90° domain switching is relatively slow, the change of P_3^{R0} always lags behind that of applied electric field E_3.

Fig. 6 shows P_3^{R0}–S_1^{R0} curves at each constant loading rate and temperature with maximum S_1^{R0} point c marked as solid circle symbols. When electric field increases in the positive x_3 direction, point c with maximum S_1^{R0} is in the region of negative P_3^{R0} at all loading rates and temperatures, being consistent with the observations of Kim et al. [13]. It is interesting to see how point c moves in the P_3^{R0}–S_1^{R0} plane with increasing loading rate or temperature. When electric field loading rate is constant, point c moves leftward and downward in the P_3^{R0}–S_1^{R0} plane with increasing temperature. When temperature is constant, point c moves upward and rightward in the plane with increasing loading rate. The movement of maximum S_1^{R0} point toward zero polarization axis with loading rate at a constant temperature was also observed by Zhou [8]. It is useful to draw two-dimensional schematic diagrams of domain distribution corresponding to each point in Fig. 6. Schematic diagrams of two-dimensional domain distribution at a typical constant temperature when electric field increases from maximum negative electric field to maximum positive electric field are shown in Fig. 7. Point a corresponds to a maximally polarized state in the negative direction at the strongest negative electric field in the figure. As an electric field at point a is reduced to zero, some domains are switched back by first step 90° switching, as discussed by Arlt et al. [25] and drawn schematically in Fig. 7(b). When electric field increases further after point b, reference remnant in-plane strain S_1^{R0} increases up to c, reaching its maximum value there. According to previous reports [26,27], most of domain switchings from b to c are first step 90° switching. It is also reported that some of the domains still remain in $-x_3$ direction at point c and thus P_3^{R0} is still negative there. After c, the domains in negative x_3 direction are switched to positive directions, mainly by second step 90° switching, thus P_3^{R0} having zero value at point d. Looking at the schematic domain distributions in Fig. 7(b), (c), and (d), which correspond, respectively, to points b, c, and d in Fig. 6, one can see first step 90° switching from b to c and second step 90° switching from c to d. As electric field continues to increase, most domains are fully polarized to positive x_3 direction at point e, as schematically shown in Fig. 7(e). The magnitude of slope of the right long-dashed straight line passing through point e is equal to that of the left straight line passing through a and b in Fig. 6, which means that only second step 90° switching occurs near point e.

An obvious comparison of the evolutions of reference remnant polarization P_3^{R0} and reference remnant in-plane strain S_1^{R0} at different temperatures can be made in schematic

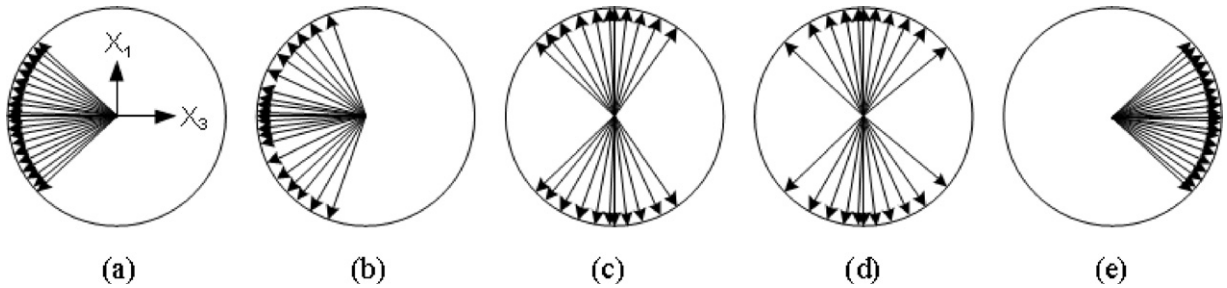

Fig. 7. Two-dimensional schematic diagrams of proposed switching process along the path from point a to point e in Fig. 3 during a typical electric field-induced polarization reversal.

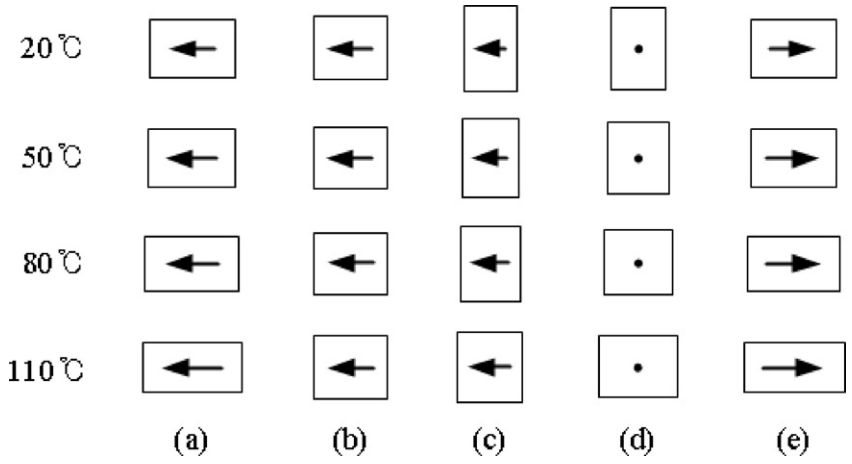

Fig. 8. One-dimensional schematic diagrams of domain switching process along the path from point a to point e in Fig. 3 at four different temperatures during electric field-induced polarization reversals.

diagrams of one-dimensional net polarization vector during polarization reversal at four different temperatures, which are shown in Fig. 8. In the figure, reference remnant polarization P_3^{R0} is represented by an arrow in a rectangular block and reference remnant in-plane strain S_1^{R0} by the height of the rectangular block. Evolutions of reference through-thickness strain S_3^{R0}, which is not measured here, can be estimated from the changes of horizontal length of schematic blocks, because domain switching process is isochoric [7] and the blocks are drawn so that their areas remain the same. At point b, where applied electric field is zero, the magnitudes of P_3^{R0} and S_1^{R0} at all four temperatures are the same at a constant loading rate of electric field, as shown in Fig. 4. Thus the sizes of blocks and arrows in Fig. 8(b) are the same independent of temperature. Points a and e correspond to maximally polarized state in negative and positive directions, respectively, having the same size of blocks and polarization arrows. At point c, S_1^{R0} is maximum and thus the height of block is the largest at a constant temperature in Fig. 8(c). At point d, the magnitude of polarization is zero, as represented by a dot symbol inside the block in Fig. 8(d). In general, the vertical height of block decreases but the horizontal length of block increases with increasing temperature, representing decreasing S_1^{R0} with temperature. The length of polarization arrow is seen to increase with temperature, which can be explained by reduced coercive field at high temperatures.

4. Conclusions

Electric displacement hysteresis and in-plane extensional strain butterfly responses of a PZT wafer under through-thickness electric field at four loading rates and four temperatures were measured and analyzed. It is observed from measurements that the magnitude of coercive field increases with increasing loading rate at a constant temperature but it decreases with increasing temperature at a constant loading rate. The magnitude of remnant polarization at zero electric field remains approximately constant at different loading rates, whereas it decreases with increasing temperature. Remnant in-plane extensional strain at zero electric field increases with increasing temperature at a constant loading rate due to thermal expansion effect; in-plane strain at a constant temperature increases with increasing loading rate over the entire range of electric field in the figure at a constant temperature.

Using piezoelectric equations and state- and temperature-dependent linear moduli of the PZT wafer, the so-called reference remnant polarization and reference remnant in-plane strain are calculated from measured electric displacement and in-plane strain. In reference remnant polarization versus electric field plots and reference remnant in-plane strain versus electric field plots, it is observed that reference remnant polarization at the states of maximum electric field increases and reference remnant in-plane strain decreases with increasing temperature at each constant loading rate. As temperature increases, the ability of electric field for driving domain switching gets larger, as indicated by reduced coercive field at high temperatures. Thus, polarization reversal is more complete at high temperatures, and as a result, most domains are polarized in the thickness direction of the wafer at maximum magnitudes of electric field. This causes smaller amount of domains arranged in in-plane directions of the wafer during polarization reversal, reducing reference remnant in-plane strain over the entire range of electric field at higher temperatures and increasing the magnitudes of reference remnant polarization at the states of maximum electric field.

It is also found that the magnitude of reference remnant polarization at the states of maximum electric field decreases and reference remnant in-plane strain over the entire range of electric field increases with increasing loading rate at each constant temperature. This effect of loading rate was explained by relatively slow 90° domain switching. 90° domain switching is relatively slow, and thus reference remnant polarization lags behind applied electric field at fast loading rates. Macroscopically, this effect leads to smaller reference remnant polarization at maximum magnitudes of electric field and larger reference remnant in-plane strain over the entire range of electric field at faster electric field loading rates.

Reference remnant polarization versus reference in-plane strain plots show that the maximum reference remnant

in-plane strain point moves downward and leftward with increasing temperature at a constant loading rate of electric field. It is also found that the maximum reference remnant in-plane strain point moves upward and rightward with increasing loading rate at a constant temperature. Two- and one-dimensional schematic diagrams of domain distribution are proposed based on 90° domain switching to illustrate domain switching processes during electric field-induced polarization reversal.

Acknowledgment

This research was supported by Basic Science Research Program through the National Research Foundation of Korea (NRF) funded by the Ministry of Education, Science and Technology (2011-0005280).

References

[1] C.M. Landis, Fully coupled, multi-axial, symmetric constitutive laws for polycrystalline ferroelectric ceramics, J. Mech. Phys. Solids 50 (2002) 127–152.
[2] J.E. Huber, N.A. Fleck, Multi-axial electrical switching of a ferroelectric: theory versus experiment, J. Mech. Phys. Solids 49 (2001) 785–811.
[3] M. Kamlah, Q. Jiang, A constitutive model for ferroelectric PZT ceramics under uniaxial loading, Smart Mater. Struct. 8 (1999) 441–459.
[4] S. Kim, A rate-dependent thermo-electro-mechanical free energy model for perovskite type single crystals, Int. J. Eng. Sci. 45 (2007) 770–785.
[5] S. Kim, A constitutive model for thermo-electro-mechanical behavior of ferroelectric polycrystals near room temperature, Int. J. Solids Struct. 48 (2011) 1318–1329.
[6] H. Cao, A.G. Evans, Nonlinear deformation of ferroelectric ceramics, J. Am. Ceram. Soc. 76 (1993) 890–896.
[7] C.S. Lynch, The effect of uniaxial stress on the electro-mechanical response of 8/65/35 PLZT, Acta Mater. 44 (1996) 4137–4148.
[8] D. Zhou, Rate dependence of soft PZT ceramics under electric field loading, Proc. SPIE Int. Soc. Opt. Eng. 4333 (2001) 64–70.
[9] M. Selten, G.A. Schneider, V. Knoblauch, R.M. McMeeking, On the evolution of the linear material properties of PZT during loading history – an experimental study, Int. J. Solids Struct. 42 (2005) 3953–3966.
[10] Q.D. Liu, J.E. Huber, State dependent linear moduli in ferroelectrics, Int. J. Solids Struct. 44 (2007) 5635–5650.
[11] Y.S. Kim, S. Kim, Evolution of linear moduli and remanent state variables during polarization reversal in a lead zirconate titanate wafer at various temperatures, Jpn. J. Appl. Phys. 50 (2011) 031503.
[12] S. Kim, Y.S. Kim, State dependent pyroelectric and thermal expansion coefficients in a PZT wafer, Ceram. Int. 36 (2010) 2189–2196.
[13] S. Kim, J.H. Kim, C. Lee, Domain switching and creep behavior of a poled PZT wafer under through-thickness electric fields at high temperatures, Acta Mater. 58 (2010) 2237–2249.
[14] S. Kim, Macroscopic comparison of ferroelectric domain switching processes in a PZT wafer at high temperatures, Cur. Appl. Phys. (2011), doi:10.1016/j.cap.2011.03.008.
[15] K.B. Chong, Thermal activation of ferroelectric switching, J. Appl. Phys. 103 (2008) 014101.
[16] A.B. Kounga, T. Granzow, E. Aulbach, High-temperature poling of ferroelectrics, J. Appl. Phys. 104 (2008) 024116.
[17] N. Wongdamnern, N. Triamnak, A. Ngamjarurojana, Y. Laosiritaworn, S. Ananta, R. Yimnirun, Comparative studies of dynamic hysteresis responses in hard and soft PZT ceramics, Ceram. Int. 34 (2008) 731–734.
[18] R.C. Smith, C.L. Hom, A temperature-dependent constitutive model for relaxor ferroelectrics, J. Intell. Mater. Syst. Struct. 16 (2005) 433–448.
[19] L.D. Mauck, Thermo-electro-mechanical behavior of ferroelectric materials. Part I: A computational micromechanical model versus experimental results, J. Intell. Mater. Syst. Struct. 14 (2003) 587–602.
[20] S. Kim, Q. Jiang, A finite element model for rate-dependent behavior of ferroelectric ceramics, Int. J. Solids Struct. 39 (2002) 1015–1030.
[21] F. Jona, G. Shirane, Ferroelectric Crystals, Pergamon Press, Oxford, 1962.
[22] P. Gerthsen, G. Kruger, Coercive field in fine-grained PLZT ceramics, Ferroelectrics 11 (1976) 489–492.
[23] N.A. Schmidt, Coercive force and 90̊ domain wall motion in ferroelectric PLZT ceramics with square hysteresis loops, Ferroelectrics 31 (1981) 105–112.
[24] G. Kruger, Domain wall motion concept to describe ferroelectric rhombohedral PLZT ceramics, Ferroelectrics 11 (1976) 417–422.
[25] G. Arlt, H. Dederichs, R. Herbiet, 90̊-domain wall relaxation in tetragonally distorted ferroelectric ceramics, Ferroelectrics 74 (1987) 37–53.
[26] T. Tsurumi, Y. Kumano, N. Ohashi, T. Takenaka, O. Fukunaga, 90̊ domain reorientation and electric-field-induced strain of tetragonal lead zirconate titanate ceramics, Jpn. J. Appl. Phys. 36 (1997) 5970–5975.
[27] N. Uchida, T. Ikeda, Temperature and bias characteristics of $Pb(Zr–Ti)O_3$ families ceramics, Jpn. J. Appl. Phys. 4 (1965) 867–880.